Evaluation of critical factors for typhoon-triggered landslide and subsequent debris flow in the Philippines using physically based models

John Christian Gaviola[1*], *Kuo* Chieh Chao[2], and *Jannet* Bencure[3]

[1]Department of Civil Engineering, Visayas State University, Baybay City, Leyte, 6521-A, Philippines
[2]Department of Civil and Infrastructure Engineering, Asian Institute of Technology, Pathum Thani, 12120, Thailand
[3]Department of Geodetic Engineering, Visayas State University, Baybay City, Leyte, 6521-A, Philippines

Abstract. This study employs physically based modeling techniques to evaluate factors that triggered the catastrophic landslide that occurred in Kantagnos Village, Baybay City, Leyte, Philippines, during Typhoon Megi in 2022. The TRIGRS and DEBRIS-2D models simulated transient infiltration effects from four days of continuous rainfall, assessing pore water pressure changes and delineating hazard zones. Parametric analyses on critical parameters—such as fstrength characteristics, soil thickness, and water table conditions—were conducted to predict spatiotemporal changes in the factor of safety. The results of the analyses indicated that the accuracy of the model could reach up to 79.23%, as evaluated by receiver operating characteristic analysis, with area zoning based on bedding plane orientation improving this by 8.23%. DEBRIS-2D effectively simulated debris flow motion and deposition areas validated against field observations. The combined use of TRIGRS and DEBRIS-2D delineated hazard zones, with 93.97% of the area within the actual debris flow boundary predicted. Key parameters, including slope geometry, material yield stress, and the quality of the digital terrain model, are crucial for predicting debris flow distance and velocity. These findings offer a valuable benchmark for developing a framework for slope disaster analysis and risk management in the region.

1 Introduction

In the past two decades, there has been a noticeable increase in the frequency and intensity of geophysical and hydrometeorological hazards, leading to severe consequences [1]. Landslides have caused significant loss of life, property, infrastructure, and economic stability. Globally, landslides caused approximately 1,000 deaths yearly, incurring an estimated USD 4 billion in damages [2]. Landslide typically refers to the swift and abrupt movement of substantial earth material, such as soil and rock debris, down a slope due to gravitational forces, often involving a clearly defined failure surface. Ali et al. [3] state that landslides occur due to conditioning and triggering factors. Conditioning factors are inherent terrain characteristics that affect the likelihood of slope failure. On the other hand, the triggering factors are external forces that prompt landslides, such as heavy rainfall, earthquakes, volcanic eruptions, and human-induced activities like deforestation and construction.

The Philippines, located in the typhoon-prone region of the Western Pacific, faces numerous natural hazards that pose significant threats to its people and infrastructure. Volcanic eruptions and earthquakes, although capable of triggering landslides, occur infrequently with long time intervals of occurrence. In contrast, landslide occurrences due to heavy and prolonged rainfall are much more common, occurring almost every month during the rainy season, and the resulting damage is frequently dealt with [4]. According to the Asian Disaster Reduction Center, about twenty typhoons enter the Philippine boundary annually, five of which are destructive. These records are equivalent to about one-fourth of the recorded events globally [5].

Given the geographical and physical characteristics of the Philippines, it is responsible for approximately 46% of the documented rainfall-induced landslides in Southeast Asia despite covering less than 10% of the total land area in the region [6]. It is challenging to model water migration in slopes with unsaturated soils, considering the influence of climate conditions [7, 8]. Intense rainfall has been shown to initiate landslides by rising pore pressure and reducing the suction of unsaturated soil on slopes [9]. Additionally, it increases the weight of the slope materials, which leads to a rise in shear stress and further destabilizes the slopes [10-12].

Access to maps that depict accurate landslide hazards and risks is crucial for identifying areas with potential landslide-related losses and effectively reducing their impact on society. To minimize the impact of landslides, it's vital to understand the factors influencing their occurrence. Various types of models have been used for slope stability evaluation. Each model has its strengths and weaknesses, with the choice of model depending on

* Corresponding author: johnchristian.gaviola@vsu.edu.ph

the specific requirements of the study, available data, and computational resources. The statistical and machine learning approaches are the most used, although they often require extensive datasets and overlook complex landslide mechanisms [13-15]. Hence, it is critical to consider susceptibility assessment from a physically based perspective, which considers the mechanical and hydrological properties and evaluates slope stability by physical laws.

This study utilized a combined physically based approach for the first time in local landslide cases and evaluated their performance for potential application in local landslide susceptibility and hazard mapping. This study primarily used the performance of the Transient Rainfall Infiltration and Grid-based Regional Slope Stability Model (TRIGRS) to evaluate the spatiotemporal variability of slope stability. The DEBRIS-2D model was used to simulate the subsequent hazard areas in case of debris flow. To use this model, the input required is the volume of the collapsed zone and its distribution. To obtain this information, the TRIGRS model was used to calculate the amount of unstable mass on a slope. These models were applied to the real slope failure cases at Kantagnos Village during Typhoon Megi in Baybay City, Leyte, Philippines. This simulation yielded the debris volume and debris depth distribution of the failure zone necessary for the flow simulation. The DEBRIS-2D model was then utilized to simulate the rapid movement of the failed mass, allowing for the evaluation of the resulting hazard zone.

The findings of this research can be a reference to establish a framework for landslide susceptibility evaluation and debris flow hazard mapping to better support disaster prevention and mitigation strategies, including the establishment of LEWS, land use policy planning, and disaster emergency response, among others. Furthermore, this work aligns with Sustainable Development Goals (SDG 11 and SDG 13): Sustainable Communities and Climate Action, by enhancing resilience and adaptive capacity to climate-related hazards and natural disasters.

2 Study area

The research was conducted on the western side of Leyte Island in the Philippines, specifically in Kantagnos Village in Baybay City. Geographically, Leyte lies in the central part of the Philippine group of islands, situated in the western Pacific Ocean (Fig. 1). Due to its location, it is highly exposed to the path of typhoons that enter the Philippine Area of Responsibility. Previous studies have identified Leyte as a region susceptible to typhoons and landslides, with the most natural disaster fatality in the country [16, 17].

The study area is located along the Anobang-Lobi Mountain range, a portion of Leyte's central mountain ranges, characterized by its rugged and mountainous terrain. It is characterized by a lithology that includes coarse conglomerate interlaced with volcanic agglomerates and breccia associated with some tuff. These characteristics arise from a series of volcanoes (Kanturao Volcanic Complex) along the central mountain range, which are inactive and extend in an NNW-SSE direction along the Philippine fault line. This geological activity has led to the island's distinct linear depressions, including elongated lakes and displaced rivers [18]. The study area has also been observed to have a bedding plane of moderately to highly weathered sandstone oriented in a southwest direction.

The study area has a Type IV climate characterized by consistent rainfall distributed throughout the year, according to the modified Corona's classification of climate provided by the state meteorological office [19]. Moreover, according to the longitudinal data provided by the Visayas State University Agrometeorological Station in Baybay City, the area has an average of about 2911 mm of precipitation annually, which peaks in December and January.

From April 8 to April 12, 2022, the study area experienced heavy rainfall due to Typhoon Megi, locally known as Typhoon Agaton. This case is highly notable as the recorded precipitation was about one-third of the average annual precipitation (996 mm). As a result, the province had several landslides and flooding events. Unfortunately, this resulted in 212 deaths, eight injuries, and 132 people reported missing. The cost of damages to agriculture, infrastructure, and houses is estimated to be at least 22.8 million USD. In Kantagnos Village alone, around 44 people were found dead, and over one hundred individuals are still missing. Fig 2 shows the 60-day antecedent rainfall profile, and Fig 3 shows the estimated rainfall intensity and maximum possible infiltration rate during Typhoon Megi in the study area. Fig 4 shows the satellite images of the landslide before and after the slope failure occurrence.

3 Methodology

This study investigated the Kantagnos landslide case by modeling pore water pressure changes, the factor of safety, and the distance and velocity of debris flow using the Typhoon Megi hydrometeorological scenario. The initial phase of this research is gathering and reviewing available data from relevant state agencies. Site observations were also conducted to gain knowledge of the actual site conditions. Moreover, laboratory testing was conducted to determine the index and engineering properties of the soils for the study area. Fig 5 shows the methodological framework for the study.

3.1 Determination of input parameters

For TRIGRS, input parameters required include soil shear strength, soil unit weight, porosity, saturated and unsaturated hydraulic conductivity, soil thickness, rainfall intensity, elevation, and slope.

The study used an IFSAR-generated DEM resampled to 5 × 5 m resolution from the Philippine National Mapping and Resources Information Authority (NAMRIA). Hydrological data were gathered from the Philippine Atmospheric, Geophysical, and Astronomical Services Administration (PAGASA).

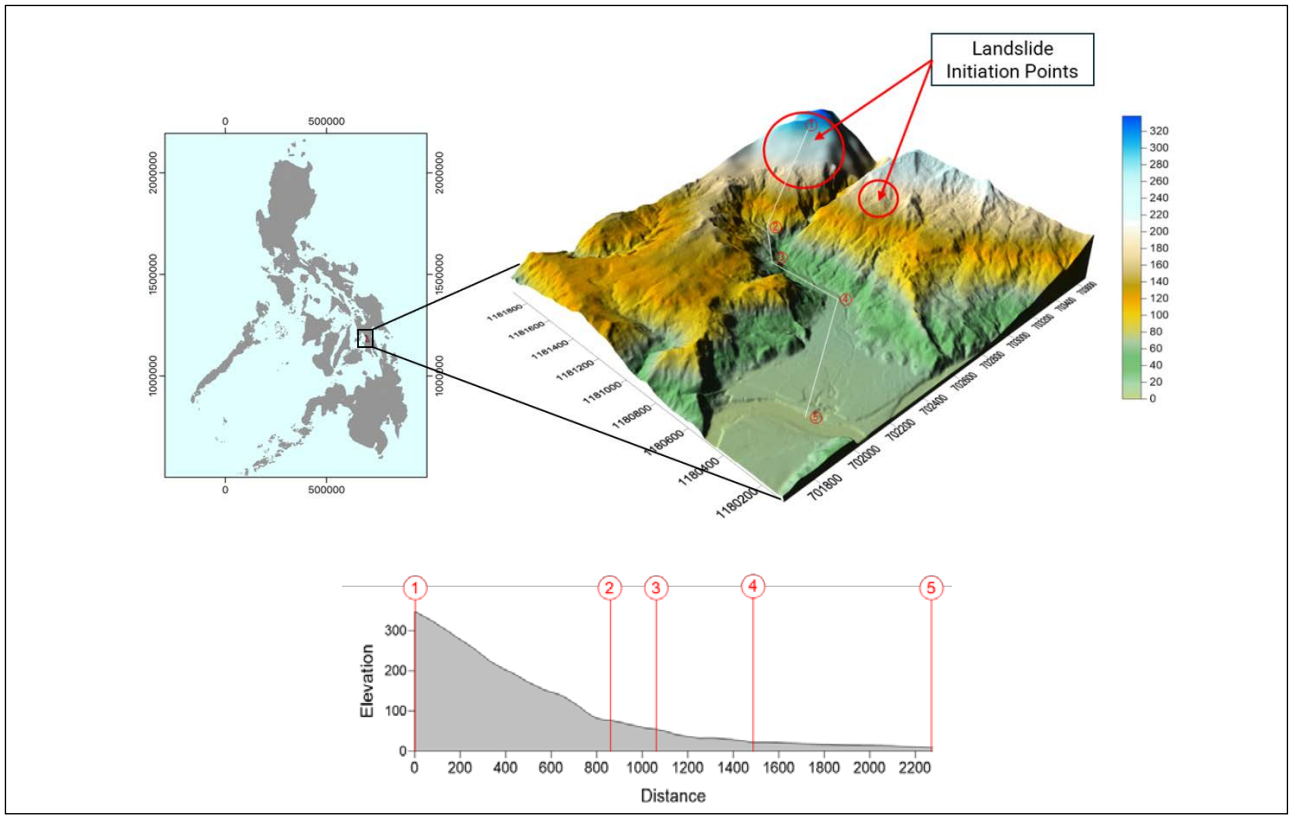

Fig. 1. Geographic and topographic attributes of the study area (data source: Phil-LiDAR)

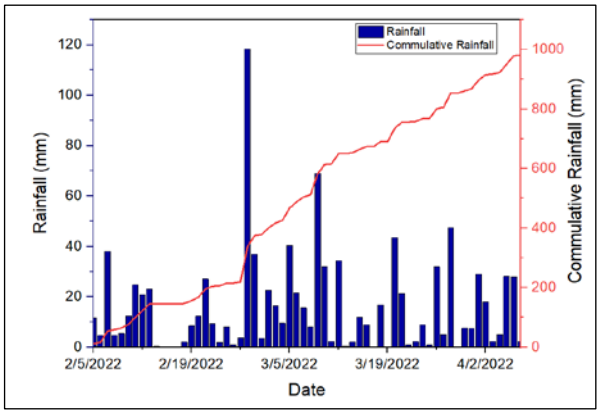

Fig. 2. 60-day antecedent rainfall data of the study area

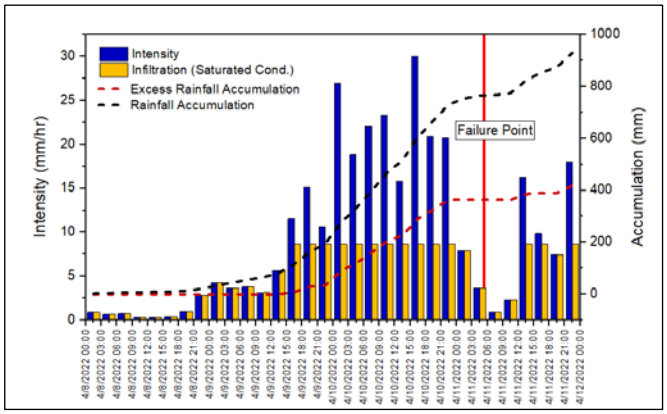

Fig. 3. Hyetograph of rainfall during Typhoon Megi

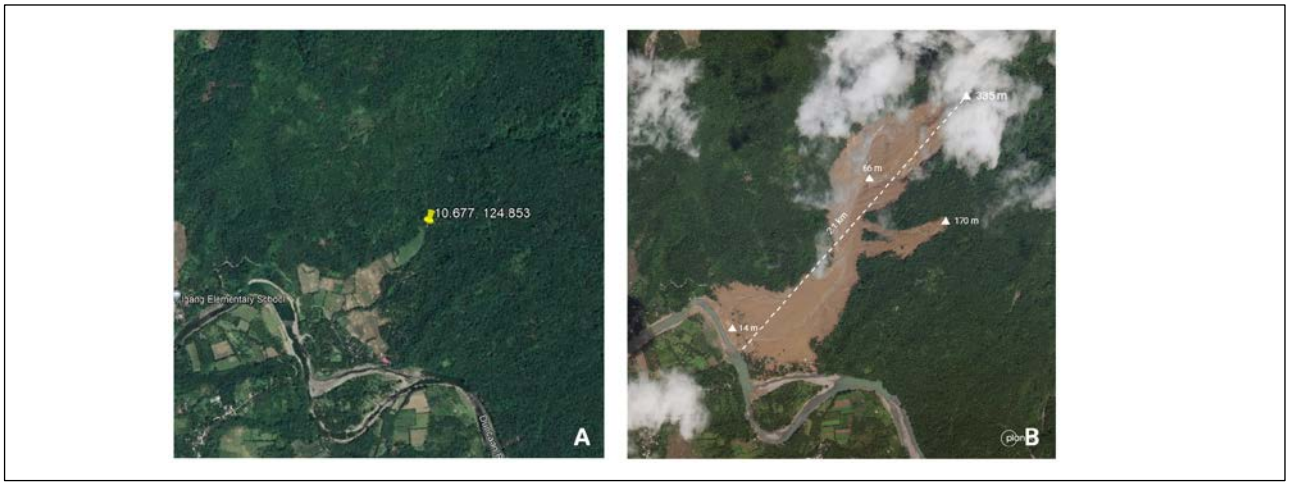

Fig. 4. Satellite images of Kantagnos Village (A) before the landslide (B) after the landslide (retrieved from https://earth.google.com, april 2024)

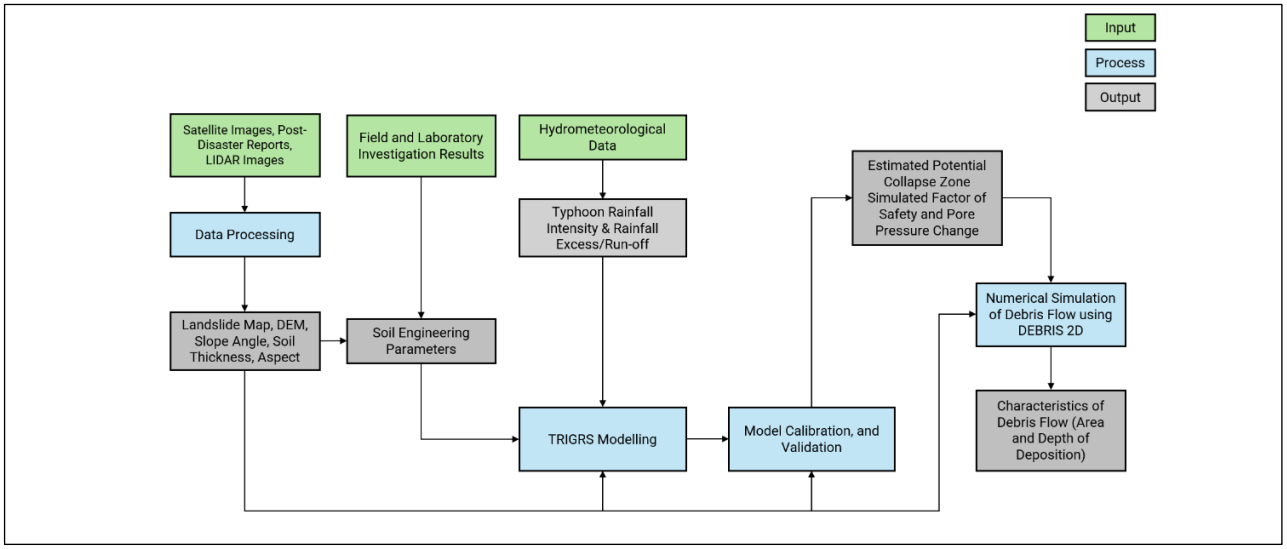

Fig. 5. Methodological framework of the study

3.2 Field investigation and laboratory testing

Field observations are essential for landslide studies as they provide firsthand data and insights into the factors contributing to landslides, their mechanisms, and potential mitigation measures. Validation of the delineated landslide/debris boundary was also conducted on-site.

The depths of the landslide at many points were also measured for soil thickness estimation. Since the model required the spatial variability of soil thickness or depth, assuming a homogeneous soil thickness would either over-estimate or under-estimate susceptibility. Unfortunately, comprehensive soil depth information was unavailable in the study area. Thus, we used the depth of the landslide scar and digital terrain models before and after the landslide to estimate soil thickness distribution. This estimation was combined with an empirical estimation suggested by Saulnier et al. [20].

A good amount of disturbed and undisturbed soil samples that were gathered from each identified sampling point were carefully transported for several laboratory tests, as follows: (1) cohesion and friction angle were determined following ASTM D3080 at a maximum strain rate of 0.0060 in/min, (2) grain size distribution were determined following ASTM D6913 and ASTM D7928, (3) Atterberg limits were determined using the ASTM D4318 standard, (4) soil moisture content, density, and specific gravity were determined based on the standard procedure ASTM 854-06, and (5) saturated hydraulic conductivity was determined following the standard procedure ASTM D5084.

The unsaturated soil parameters required to build the Soil-Water Characteristic Curve (SWCC) were determined through empirical equations from previous studies. Many successful studies in the past using physically based models have only been estimated based on previous studies, primarily based on the grain size distribution [21-23]. For this study, the alpha value, the saturated volumetric water content (θ_s), and residual volumetric water content (θ_r) were estimated following the Van Genuchten water retention curve using the ROSETTA 3 Lite Module [24]. Moreover, the value of diffusivity, D_0, was estimated based on the commonly used empirical equation of Liu and Wu [25], $D_0 = 200K_s$. The input parameters are summarized in Table 1.

A satellite precipitation dataset was also used to supplement the field rain gauge data. The GPM IMERG daily "final" precipitation is available at half-hourly, 3-hourly, daily, and monthly intervals on their website: *https://gpm.nasa.gov/data/source*. For this study, a 3-hour rainfall intensity interval was used in the simulation of a 77-hour typhoon for computational efficiency reasons.

3.3 Spatial data processing

The TRIGRS and DEBRIS-2D models require a high-quality digital elevation model (DEM) of the area before a landslide event. This study used a DEM with a 5-m resolution, which was then processed to create slope and flow direction maps. The DEM was also used for hydrological modeling, which includes predicting the direction and accumulation of water flow.

3.4 TRIGRS model

The TRIGRS Model is designed to model the timings and distribution of shallow landslides caused by rainfall [26]. It determines transient shifts in pore pressure and changes in the factor of safety resulting from rainwater infiltration. It models infiltration, covering events lasting from hours to days, using analytical solutions to partial differential equations that describe one-dimensional vertical water flow in saturated or unsaturated homogeneous and isotropic materials.

The factor of safety (FS) at a depth of Z at any time, t, is then calculated using the following equation:

$$FS(Z,t) = \frac{tan\varphi'}{tan\theta} - \frac{c' - (\psi(Z,t)\rho_w tan\varphi')}{\rho Z sin\theta cos\theta} \quad (1)$$

where φ' denotes the soil's internal friction angle, θ represents the slope angle, c' is the effective soil cohesion,

ρ_w stands for the unit weight of water, and ρ indicates the total unit weight of soil.

Equations 2 and 3 provide linearized solutions of the Richards equation by Iverson [27] to express groundwater head, φ, when there is an impermeable basal boundary at a finite depth:

$$\varphi(Z,t) = [Z-d]\beta + 2\sum_{n=1}^{N}\frac{I_{nz}}{K_z}H(t-t_n)[D_1(t-t_n)]^{\frac{1}{2}}\sum_{m=1}^{\infty}\left\{\begin{array}{l} ierfc\left[\frac{(2m-1)d_{LZ}-(d_{LZ}-Z)}{2[D_1(t-t_n)]^{\frac{1}{2}}}\right] \\ +ierfc\left[\frac{(2m-1)d_{LZ}+(d_{LZ}-Z)}{2[D_1(t-t_n)]^{\frac{1}{2}}}\right]\end{array}\right\} - 2\sum_{n=1}^{N}\frac{I_{nz}}{K_z}H(t-t_{n+1})[D_1(t-t_{n+1})]^{\frac{1}{2}}\sum_{m=1}^{\infty}\left\{\begin{array}{l} ierfc\left[\frac{(2m-1)d_{LZ}-(d_{LZ}-Z)}{2[D_1(t-t_{n+1})]^{\frac{1}{2}}}\right] \\ +ierfc\left[\frac{(2m-1)d_{LZ}+(d_{LZ}-Z)}{2[D_1(t-t_{n+1})]^{\frac{1}{2}}}\right]\end{array}\right\} \quad (2)$$

$$ierfc(\eta) = \frac{1}{\sqrt{\pi}}\exp(-\eta^2) - \mu erfc(\eta) \quad (3)$$

where t is the time variable, $Z = z/\cos\theta$ is a special variable in vertical coordinate direction, d is the initial, depth of the water table measured in Z direction in steady state, d_{LZ} means the depth of an impermeable basal boundary, $\beta = \lambda \cos\theta$, where $\lambda = \cos\theta - (I_z/K_z)_{LT}$, and in which K_z is a hydraulic conductivity, Iz is an initial surface flux, I_{nz} is a surface flux of a given intensity in nth time I, D_0 is the saturated hydraulic conductivity.

To handle varying rainfall intensities, the program utilizes a step-function series. It features a straightforward runoff routing model, which allows users to channel excess water from impermeable zones to more permeable areas further downslope. Each cell's factor of safety calculations uses a clear-cut infinite-slope model. The program accounts for horizontal heterogeneity by enabling differences in material properties, rainfall patterns, and other parameters across individual cells. The components of the TRIGRS model are detailed in Fig 6.

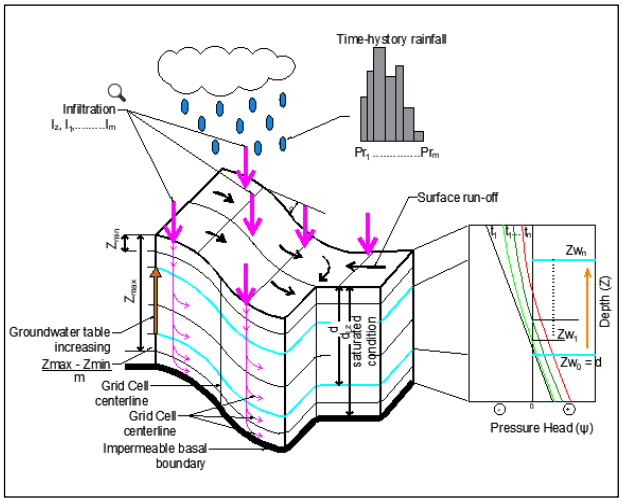

Fig. 6. Components of the TRIGRS model in finite impermeable boundary conditions (modified from Grelle et al., 2013)

Table 1. TRIGRS model input parameters

Parameter	Unit	Values	Reference
Slope	degree	variable	DEM
Soil Thickness	m	variable	Saulnier et al. (1997)
Unit Weight,	g/cc	1.66 to 1.86	Laboratory Testing
Specific Gravity		2.55 to 2.56	Laboratory Testing
Cohesion, c	kPa	24.04 to 42.63	Laboratory Testing
Friction Angle, φ	degrees	15.86 to 20.43	Laboratory Testing
Saturated Hydraulic Conductivity, K_s	cm/s	3.5×10^{-4} to 1.3×10^{-4}	Laboratory Testing
Saturated volumetric water content (θ_s)	m^3/m^3	0.378	Estimation of SWCC parameters using the ROSETTA 3 Module (Schaap et al., 2001, Zhang and Schaap, 2017)
Residual volumetric water content (θ_r)	m^3/m^3	0.067	
Pore-size parameter, α	1/m	2.073	
Saturated hydraulic diffusivity (D_0)	m^2/s	4.8×10^{-4}	Estimation from Liu and Wu (2008)
Steady infiltration rate, I_z	m s^{-1}	0.01K_s	Salciarini et al., 2008; Liu and Wu, 2008; Kim et al., 2010; Park et al., 2013
Hydraulic diffusivity, D_0	m^2 s^{-1}	200 K_s	Liu and Wu (2008)
Soil Depth, S_t	m	Varied	Saulnier et al. (1997)
Initial Water Depth, W_d	m	0-100% of soil thickness	Salciarini et al. (2007)

3.5 Analysis of rainfall infiltration induced shallow landslide

3.5.1 Model calibration

To maintain the reliability of our model, a calibration process was carried out to ensure input parameters are confined within a realistic range. This calibration involves performing a sensitivity analysis to determine the most relevant inputs. Studies have recommended the evaluation of several parameters, including the initial groundwater condition (wt), cohesion (c), and internal angle of friction (φ) [15, 28, 29]. This was adopted in the study by calibrating the model using the range of values of these parameters from the field and laboratory observations. Meanwhile, the values for the water table were varied by percentage of the soil thickness following Salciarini et al. [30] as the water table remains unknown in this case. The accepted trials are compared based on their error indices to optimize the reliability of the results.

3.5.2 Model evaluation and validation

The model's performance was evaluated using a confusion matrix and a receiver operating characteristic (ROC) curve. Each cell in the simulation result falls into one of four categories: true positive (TP) when the model

correctly predicts instability for a landslide source, false negative (FN) when it incorrectly assesses the same cell as stable, true negative (TN) when it accurately identifies stable cells, and false positive (FP) when it wrongly predicts instability. Key evaluation metrics include sensitivity (TPR), which measures the proportion of correctly identified positives, and specificity (TNR), which measures the proportion of true negatives. Balanced Accuracy, the mean of TPR and TNR, is used to handle imbalanced data, with its complement termed the error index. The ROC curve was created using TPR and FPR values at various cut-off points, with the area under the curve (AUC) interpreted according to Yesilnacar and Topal [31].

3.6 DEBRIS-2D model

Unstable hillsides with FS less than 1.0 can collapse rock and soil, which can combine with water to form a debris flow downslope. This model considers debris flow as a non-Newtonian fluid that has yield stress. It can calculate the velocity and depth of the flow, the affected area, and the impact force over time. The DEBRIS-2D model is a simulation tool used to replicate numerous debris flow events in different parts of the world, primarily focusing on cases in Taiwan and other Asian countries. The results match well with field observations such as the study of Tsai et al. [32], Wu et al. [33], and Hsu and Liu [34].

The following text describes a mathematical model developed by Liu and Huang [35] which is designed to calculate using the conservation of mass and momentum laws for long waves in the plug flow region. DEBRIS-2D uses an inclined coordinate system where the x-axis aligns with the flow direction, the y-axis aligns with the topographical contour direction, and the z-axis points to the depth direction at the x-y plane. The velocity components of an object moving in the x and y directions are denoted as u and v, respectively. The inclination angle is represented by θ, while the yield stress is defined by τ_0, and H represents the flow depth, calculated as the difference between the free surface (h) and the natural bottom of the debris flow (B). The momentum and continuity equations are expressed in conservative form as Equations 4, 5, and 6, respectively.

$$\frac{\partial uH}{\partial t}+\frac{\partial u^2H}{\partial x}+\frac{\partial uvH}{\partial y}=-gcos\theta H\frac{\partial(B+H)}{\partial x}+gsin\theta H-\frac{1}{\rho}\frac{\tau_0 u}{\sqrt{u^2+v^2}} \quad (4)$$

$$\frac{\partial vH}{\partial t}+\frac{\partial uvH}{\partial x}+\frac{\partial v^2H}{\partial y}=-gcos\theta H\frac{\partial(B+H)}{\partial y}-\frac{1}{\rho}\frac{\tau_0 v}{\sqrt{u^2+v^2}} \quad (5)$$

$$\frac{\partial H}{\partial t}+\frac{\partial uH}{\partial x}+\frac{\partial vH}{\partial y}=0 \quad (6)$$

3.7 Subsequent motion of collapsed mass

3.7.1 Model scenarios

Two cases of simulations were run for this study. The first scenario was based on the actual site conditions where the source information was derived from the difference between the DTM before and after the landslide occurred, with the yield stress varying from 300 Pa to 700 Pa, as recommended by Wu et al. [33] for sand with mud debris materials. The second case used the results of the TRIGRS and the back-calculated yield stress value from the first scenario. The input parameters for debris flow simulation are detailed in Table 2.

Table 2. DEBRIS-2D model input parameters

Parameters	**Input Value**
Elevation	Digital Elevation Model (5x5 m)
Simulation Range	700874.182731 - 703874.182731 E 1179367.29761 - 1182057.29761 N
Mass Volume	Case 1: Estimated actual volume Case 2: TRIGRS model predicted
Unit Weight	1.76 g/cc (Laboratory Testing)
Geometry	Length characteristics of landslide Elevation difference characteristics Depth characteristics of the mass source
Yield Stress	Parametric Analysis: 300 -700 Pa “Sand with Mud” material [33]

3.7.2 Model evaluation and validation

The simulation results were evaluated by comparing them with actual field observations and aerial photographs. The affected area, which includes initiation, transportation, and deposition zones, as well as the deposition depth from the simulation, were assessed with the in-situ observations to determine the accuracy of the simulation [34]. The yield stress value that generates the least error (% overestimation and % missed) is considered the most probable value.

4 Results and discussion

4.1 Slope stability modeling

The parametric analyses were conducted in multiple sets, the first and second of which were designed to eliminate the least probable values and reduce the number of additional trial simulations for more detailed parameter values. The parametric analysis reveals that the trial combination of φ = 16°, c = 32 kPa, wt = 20% of soil thickness would give a more realistic result with the least error of around 20.77%. This means that about 79 pixels in every 100 pixels within the landslide boundary were correctly predicted; likewise, about 79 pixels in every 100 pixels outside the landslide boundary were also correctly predicted.

Likewise, parametric analysis, reveals that the initial water table of 20% of the soil thickness gives the least error in predicting the landslide initiation area. This is relatively high already for sloping ground or mountainous regions. This could be attributed to the high antecedent rainfall (60-day rainfall data), with 68.38% and 188.82% increase from the long-term average monthly rainfall for February and March 2022, months before the slope failure occurrence, respectively.

The TRIGRS model uses a zonation technique to improve accuracy and reduce overestimation. The study area is zoned based on the slope aspect relative to the bedding plane direction. Areas with a cataclinal bedding-

slope relationship, where the slope aligns with the bedding plane, are at higher landslide risk. The application of zoning resulted in increased performance in terms of predicting the stable area while maintaining a good prediction of the actual unstable area (refer to Fig. 7). Result shows that true negative rate (TNR) increased from 75.59% to 93.18%, consequently decreasing the false positive rate (FPR) by 17.59% from the former model. Furthermore, the model prediction accuracy has improved by 8.21% from 79.23% to 87.44%.

Figure 8 shows the change in the predicted unstable area with time from the start of the typhoon up to the estimated time of failure about 77 hours later. The landslide source is only about 7.10% (94,575 m^2) of the total area considered in the study.

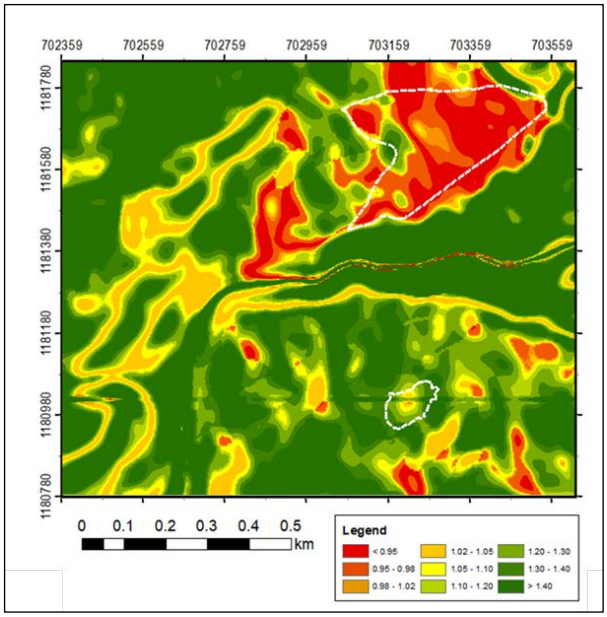

Fig. 7. Spatial model of the simulated factor of safety at the time of failure

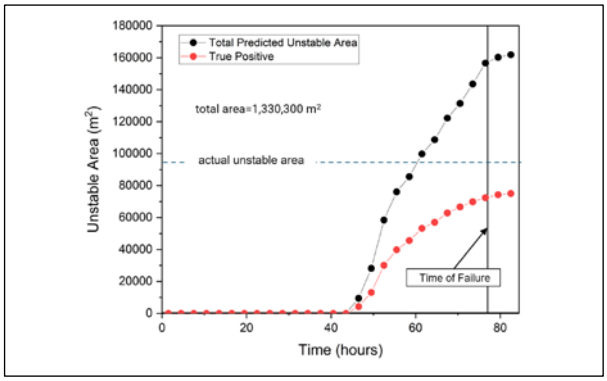

Fig. 8. Temporal change of predicted unstable area (FS<1.0)

4.1.1 Pressure head and factor of safety response

At the onset of the typhoon, low rainfall intensity maintained a steady state for up to 12 hours, with the pressure head nearly matching a hydrostatic distribution (Fig. 9a). As rainfall intensity increased, surface flux (I_{nz}) rose, leading to infiltration. This caused an increase in β and the transient terms of the TRIGRS model, raising the pressure head. After 36 hours of infiltration and 80 mm of rainfall, a gradual change in pressure head occurred, as infiltration in the unsaturated zone remained limited until it interacted with the water table. Fig. 9b illustrates the factor of safety response with depth at a representative slope point.

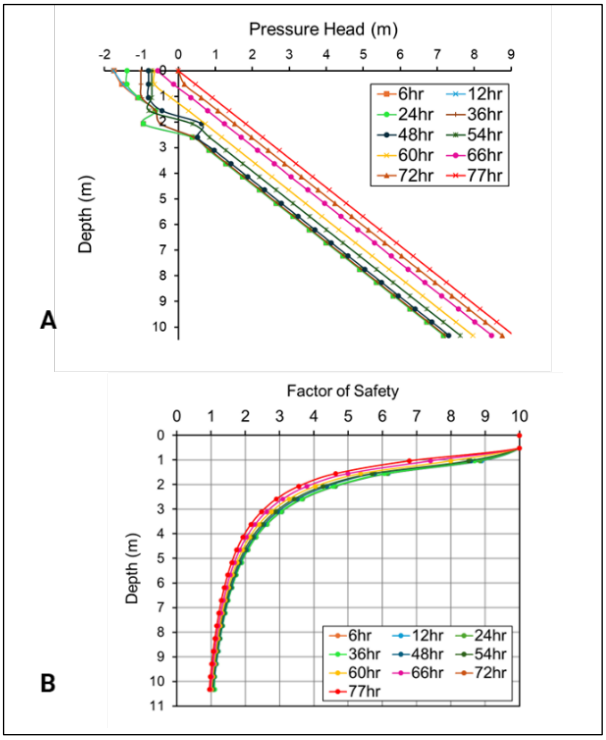

Fig. 9. (a) Temporal of the pressure head and (b) the factor of safety with depth taken at a representative point of average slope

Infiltration increases the groundwater's pressure head, lowering safety factor values and leading to slope instability (FS < 1.0). The analysis showed that slope failure occurred where the angle was $\theta \geq 16.70^{o}$, but only on slopes up to 25.18º. As the slope angle increases, soil thickness decreases, reducing the maximum pressure head at the base of the soil layer. While the driving force increases with slope, the decrease in resisting force due to pressure head is less significant, maintaining stability up to a certain slope angle. Figure 10 illustrates the corresponding change in the factor of safety as a response to the change in the pore pressure at different time.

4.1.2 Validation of the spatial model

The TRIGRS model was validated using the Area Under the Curve (AUC) metric. The results of the validation are presented in Fig. 11. It reveals a strong predictive capability with an AUC value of 0.885, indicating "very good performance" according to Yesilnacar and Topal [25]. A True Positive Rate (TPR) of 74.77% and a True Negative Rate (TNR) of 92.41% further confirm the model's reliability in identifying landslide and non-landslide areas. The False Positive Rate (FPR) of 7.59% and False Negative Rate (FNR) of 25.23% highlight the model's low rate of misclassification. These metrics demonstrate the TRIGRS model's reliability for landslide prediction and risk assessment.

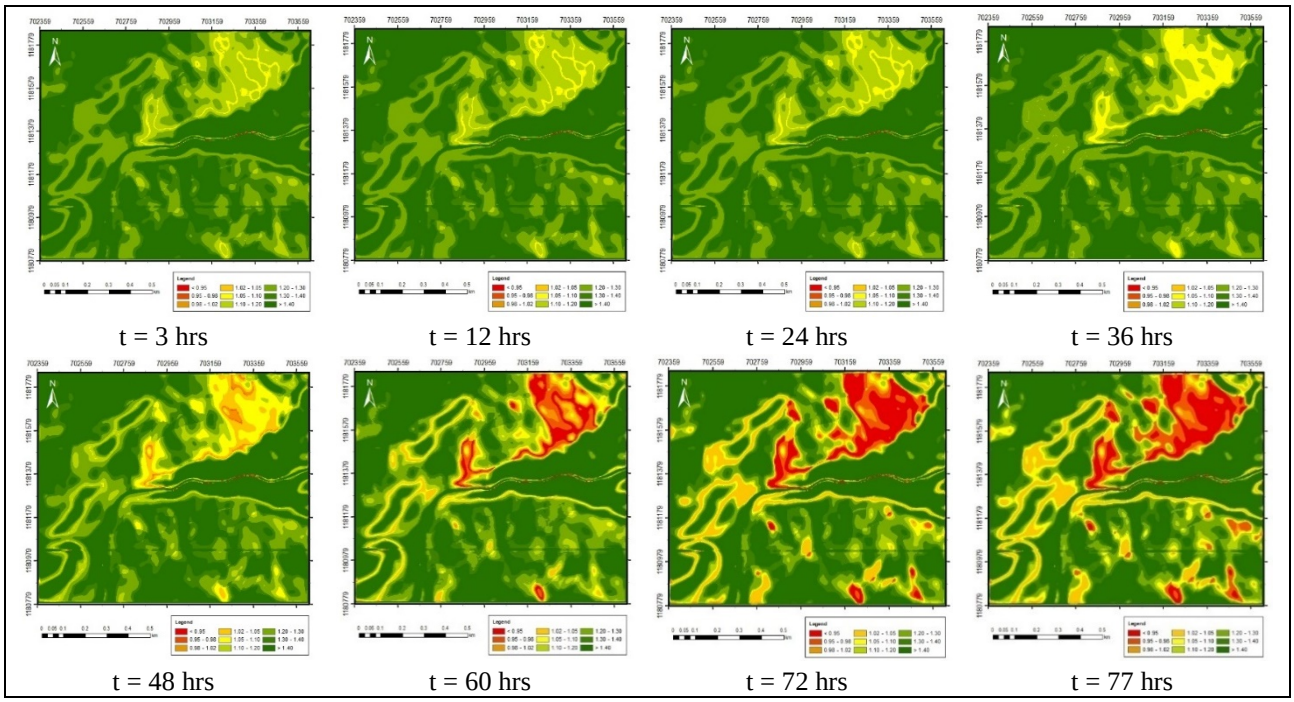

Fig. 10. Change of total unstable area (FS<1.0) across space and time

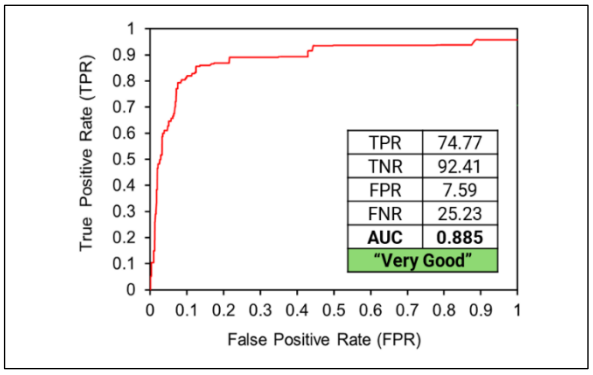

Fig. 11. Performance of the TRIGRS model in terms of the TPR and FPR, and the area under the receiver-operating characteristic curve (AUC)

4.1.3 Debris flow motion

To estimate debris arrival timing in the village, specific house/building locations were marked as benchmarks in the model. Three points shown in Fig. 12 were evaluated, with debris traveling over 2 km. in 2 minutes. Points 1, 2, and 3, located 1630 m, 1795 m, and 2130 m from the landslide initiation point, are estimated to be reached at 56, 87, and 109 seconds, respectively. Fig. 13 shows debris spread and depth at various times. Disaster survivors confirmed these timings as reasonable.

The temporal variations in maximum velocity and debris flow depth at four monitoring locations were also investigated in the model through arbitrary monitoring points. These points placed along the debris flow path and deposition zones near former residential areas, help simulate and validate findings, as in Wu et al. [33].

These observations underscore the importance of considering both velocity and depth when assessing the debris flow risks and highlight how monitoring key points along the flow path provides valuable insights into their destructive potential.

4.1.4 Validation of Debris flow modeling results

The final debris depth at the deposition zone, estimated by the DEBRIS-2D model, is shown in Fig. 14. Among the affected structures, Kantagnos Elementary School and several residential houses were reached by debris but remained unmoved, serving as benchmarks for validating the model. The school was buried under 2.5 meters of debris, while the model predicted a depth of 2.0 - 3.0 meters, aligning with actual measurements. The model also accurately predicted the debris depth around a residential house (2.5 - 3.0 meters) and correctly indicated that the Kantagnos Auditorium used as an evacuation site, was not affected by debris.

4.2 Combined TRIGRS and DEBRIS-2D models in landslide hazard zone mapping

The hazard zone predicted by the combined TRIGRS-DEBRIS-2D modeling is shown in Fig. 15, with the evaluation results summarized in Table 3. As shown, the combined model accurately delineated 93.97% of the 1,281,484 sq. meters of the hazard area, highlighting its strong ability to identify landslide-prone zones. By integrating TRIGRS, which predicts landslide initiation, and DEBRIS-2D, which models debris flow extent, the approach offers a comprehensive method for hazard mapping. While the model is effective, fine-tuning parameters such as soil thickness, initial water table, and precipitation patterns could improve accuracy, reducing overestimation and mispredictions.

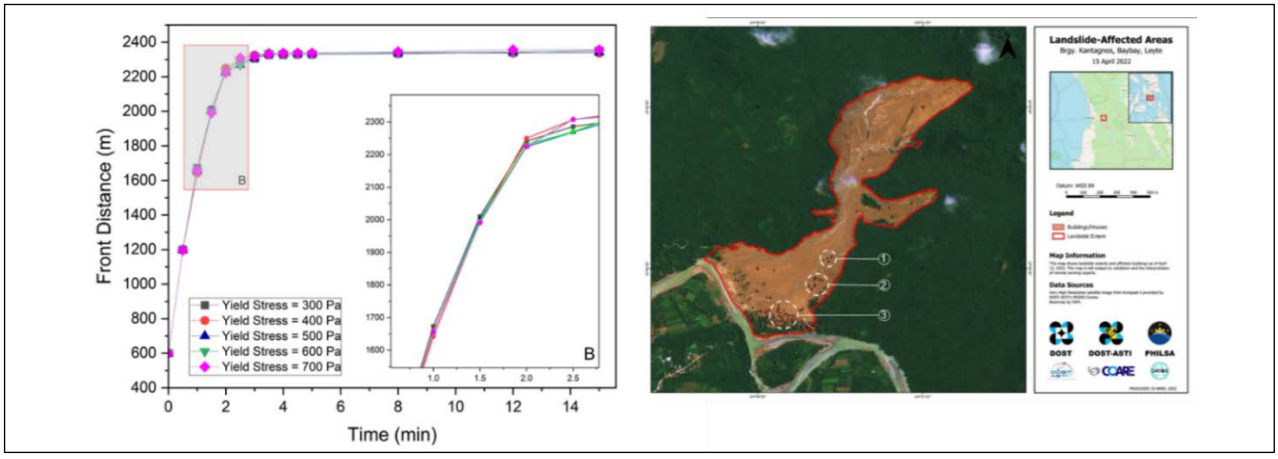

Fig. 12. Estimated time of arrival of debris as simulated by DEBRIS-2D (distance of Points 1, 2, and 3 are around 1630m, 1795, and 2130m, respectively, measured from the top of the debris source) (image source: DOST)

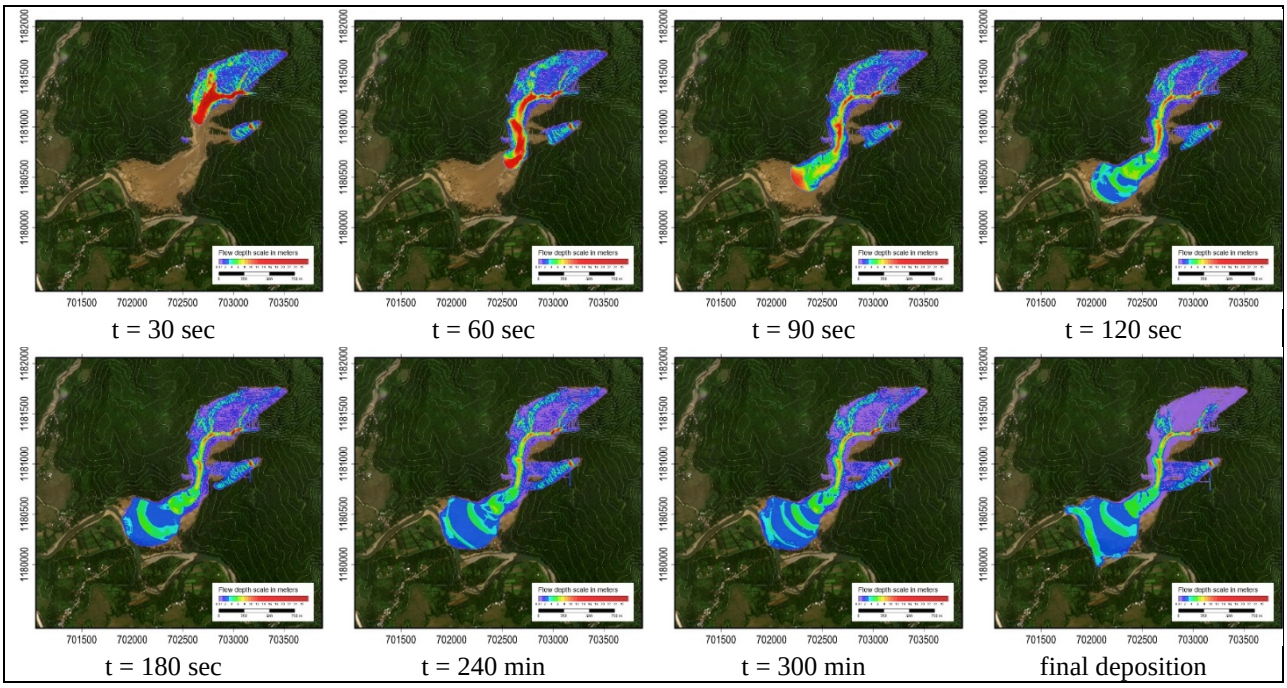

Fig. 13. Spatiotemporal change of the debris flow front and deposition depth

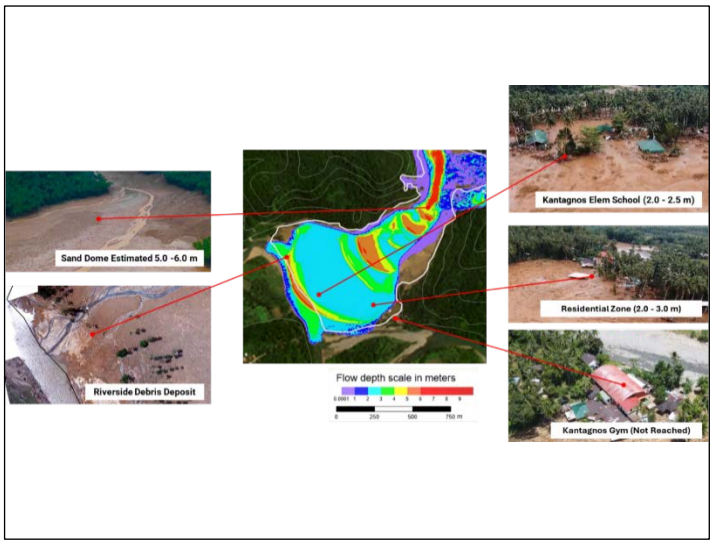

Fig. 14. Validation of the simulated debris deposition depth

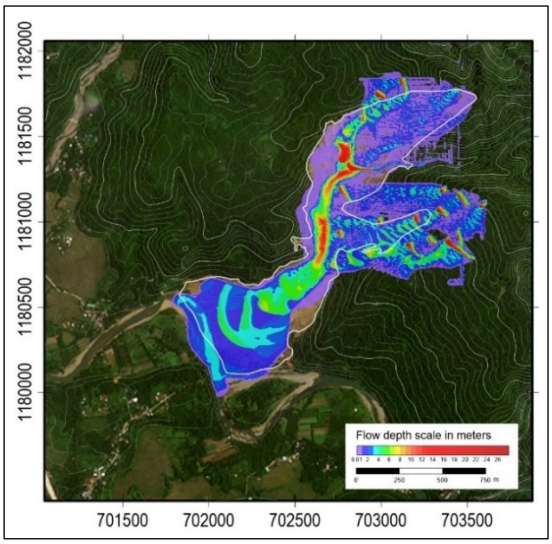

Fig. 15. Combined TRIGRS-DEBRIS-2D modeling

Table 3. Performance of the combined TRIGRS and DEBRIS-2D models

Delineated Hazard Area (sq.m)	% Matched (Correct Prediction)	% Over-estimation (Overprediction)	% Missed (Under-prediction)
1,281,484	93.97%	37.70%	6.42%

5 Conclusion

This study evaluates the performance of the TRIGRS and DEBRIS-2D models in analyzing slope stability and debris flow during a rainfall-induced landslide in Kantagnos Village, Baybay City, Leyte, Philippines. Parametric analyses improved simulation accuracy, with the best results using $\varphi = 16°$, $c = 32$ kPa, and a water table depth of 20% of the soil thickness, achieving a 20.77% prediction error and 79.23% balanced accuracy. Zoning based on bedding plane orientation increased the true negative rate from 75.59% to 93.18%, improving overall accuracy by 8.23%. The study emphasized the importance of the initial water table in landslide initiation, identifying a critical threshold of 0.35 times the soil thickness, which could inform early warning systems. The TRIGRS model effectively simulated rainfall infiltration and landslide dynamics, while DEBRIS-2D accurately modeled debris flow using yield stress of 500 Pa. Together, the models correctly predicted 93.97% of the debris flow boundary, demonstrating their strength in hazard mapping.

For future research, it is recommended to integrate geophysical methods for accurate soil thickness mapping, conduct long-term groundwater monitoring, study the impact of weathering on shear strength parameters, explore additional zoning techniques, and compare TRIGRS and DEBRIS-2D with other models for improved accuracy and cost-effectiveness.

This work was supported by the Department of Science and Technology – Science Education Institute (DOST-SEI) of the Republic of the Philippines, the Asian Institute of Technology (AIT, Thailand), and the Visayas State University (VSU, Philippines) under the Internationalization Program (IP) Research Grant VSU-IP-2023-7.

References

1. G. Rahman et al., Assessment of landslide susceptibility, exposure, vulnerability, and risk in Shahpur Valley, Eastern Hindu Kush, Front Earth Sci (Lausanne), **10,** (2022). https://doi.org/10.3389/feart.2022.953627
2. B. Pradhan and A. M. Youssef, Manifestation of remote sensing data and GIS on landslide hazard analysis using spatial-based statistical models, Arabian Journal of Geosciences, **3**(3), 319–326 (2010). https://doi.org/10.1007/s12517-009-0089-2
3. S. Ali, P. Biermanns, R. Haider, and K. Reicherter, Landslide susceptibility mapping by using a geographic information system (GIS) along the China-Pakistan Economic Corridor (Karakoram Highway), Pakistan, Natural Hazards and Earth System Sciences, **19**(5), 999–1022, (2019). https://doi.org/10.5194/nhess-19-999-2019
4. D. Nolasco-Javier and L. Kumar, Deriving the rainfall threshold for shallow landslide early warning during tropical cyclones: a case study in northern Philippines, Natural Hazards, **90**(2), 921–941 (2018). https://doi.org/10.1007/s11069-017-3081-2
5. M. G. A. Huigen and I. C. Jens, Socio-Economic Impact of Super Typhoon Harurot in San Mariano, Isabela, the Philippines, World Dev, **34**(12), 2116–2136, (2006). https://doi.org/10.1016/j.worlddev.2006.03.006
6. M. J. Froude and D. N. Petley, Global fatal landslide occurrence from 2004 to 2016, Natural Hazards and Earth System Sciences, **18**(8), 2161–2181, (2018). https://doi.org/10.5194/nhess-18-2161-2018
7. K. C. Chao, J. B. Kang, and J. D. Nelson, Challenges in water migration modeling for expansive soils. GeoShanghai Conference, Shanghai, China, 204–213 (2014).
8. K. C. Chao, J. B. Kang, J. D. Nelson, Evaluation of failure of embankment slope constructed with expansive soils, Geotechnical Engineering Journal of the SEAGS & AGSSEA, **49**(2), 140-149 (2018).
9. W. H. Schulz, J. P. McKenna, J. D. Kibler, and G. Biavati, Relations between hydrology and velocity of a continuously moving landslide-evidence of pore-pressure feedback regulating landslide motion?, Landslides, **6**(3), 181–190, (2009). https://doi.org/10.1007/s10346-009-0157-4
10. J. Mathew, D. G. Babu, S. Kundu, K. V. Kumar, and C. C. Pant, Integrating intensity-duration-based rainfall threshold and antecedent rainfall-based probability estimate towards generating early warning for rainfall-induced landslides in parts of the Garhwal Himalaya, India, Landslides, **11**(4), 575–588, (2014). https://doi.org/10.1007/s10346-013-0408-2
11. T. Amarathunga, K. C. Chao, and J. D. Nelson, Effect of climate change on rainfall-induced failures for embankment slopes in Timor-Leste. Proceedings of the 20th International Conference on Soil Mechanics and Geotechnical Engineering, Sydney, Australia, 2341–2347, (2022).
12. P. Morya, S. Kongpanickul, K. C. Chao, and R. Ishenaliev, Rainfall-induced failure on unsaturated fill and highly weathered Schist slopes. The 7th Asia-Pacific Unsaturated Soils Conference, Nagoya, Japan, **7**(2), 556–564, (2019).
13. J. L. Zêzere, S. Pereira, R. Melo, S. C. Oliveira, and R. A. C. Garcia, Mapping landslide susceptibility using data-driven methods, Science of the Total Environment, **589,** (2017). https://doi.org/10.1016/j.scitotenv.2017.02.188
14. S. Zhang, L. Zhao, R. Delgado-Tellez, and H. Bao, A physics-based probabilistic forecasting model for rainfall-induced shallow landslides at regional scale, Natural Hazards and Earth System Sciences, **18**(3),

969–982, (2018). https://doi.org/10.5194/nhess-18-969-2018

15. V. Medina, M. Hürlimann, Z. Guo, A. Lloret, and J. Vaunat, Fast physically-based model for rainfall-induced landslide susceptibility assessment at regional scale, Catena (Amst), **201,** (2021). https://doi.org/10.1016/j.catena.2021.105213
16. J. Gray, S. Lloyd, S. Healey, and A. Opdyke, Urban and rural patterns of typhoon mortality in the Philippines, Progress in Disaster Science, **14**(100234), (2022). https://doi.org/10.1016/J.PDISAS.2022.100234
17. G. D. C. Santos, 2020 Tropical cyclones in the Philippines: A review, Tropical Cyclone Research and Review, **10**(3), 191–199, (2021). https://doi.org/10.1016/j.tcrr.2021.09.003
18. R. N. Eco et al., Journal of the Philippine Geoscience and Remote Sensing Society (2015). Available: http://philgrss.org/journal/
19. PAGASA. Climate Change in the Philippines. Philippine Atmospheric, Geophysical and Astronomical Services Administration. (2011).
20. G. M. Saulnier, K. Beven, and C. Obled, Including spatially variable effective soil depths in TOPMODEL, J Hydrol (Amst), **202**(1–4), 158–172 (1997). https://doi.org/10.1016/S0022-1694(97)00059-0
21. F. de Luiz Rosito Listo, M. C. Villaça Gomes, and F. S. Ferreira, Evaluation of shallow landslide susceptibility and Factor of Safety variation using the TRIGRS model, Serra do Mar Mountain Range, Brazil, J South Am Earth Sci, **107**, (2021). https://doi.org/10.1016/j.jsames.2020.103011
22. G. Grelle et al., Space-time prediction of rainfall-induced shallow landslides through a combined probabilistic/deterministic approach, optimized for initial water table conditions, Bulletin of Engineering Geology, and the Environment, **73**(3), 877–890 (2014). https://doi.org/10.1007/s10064-013-0546-8
23. L. Schilirò, J. Cepeda, G. Devoli, and L. Piciullo, Regional analyses of rainfall-induced landslide initiation in upper gudbrandsdalen (South-eastern Norway) using TRIGRS model, Geosciences (Switzerland), **11**(1), 1–15, (2021). https://doi.org/10.3390/geosciences11010035
24. Y. Zhang and M. G. Schaap, Weighted recalibration of the Rosetta pedotransfer model with improved estimates of hydraulic parameter distributions and summary statistics (Rosetta3), J Hydrol (Amst), **547**, 39–53, (2017). https://doi.org/10.1016/j.jhydrol.2017.01.004
25. C. N. Liu and C. C. Wu, Mapping susceptibility of rainfall-triggered shallow landslides using a probabilistic approach, Environmental Geology, **55**(4), 907–915, (2008). https://doi.org/10.1007/s00254-007-1042-x
26. R. L. Baum, W. Z. Savage, and J. W. Godt, TRIGRS-A Fortran Program for Transient Rainfall Infiltration and Grid-Based Regional Slope-Stability Analysis, Version 2.0, [Online]. Available: http://geohazards.cr.usgs.gov/
27. R. M. Iverson, Landslide triggering by rain infiltration," Water Resour Res, **36**(7), 1897–1910, (2000). https://doi.org/10.1029/2000WR900090
28. M. Hürlimann, Z. Guo, C. Puig-Polo, and V. Medina, Impacts of future climate and land cover changes on landslide susceptibility: regional scale modelling in the Val d'Aran region (Pyrenees, Spain), Landslides, **19**(1), 99–118, (2022). https://doi.org/10.1007/s10346-021-01775-6
29. A. Parapan, K. C. Chao, K. Saowiang, S. Soralump, and T. Nontapot, Evaluation of key parameters in rainfall-induced shallow landslide analysis: Are Di Village case, IOP Conference Series: Earth and Environmental Science, **1334**(1), 012015, (2024). https://doi.org/10.1088/1755-1315/1334/1/012015
30. D. Salciarini, C. Tamagnini, F. Ronchi, E. Volpe, and G. Fanelli, An approach for large-scale soil characterization for the application of non-structural landslide risk mitigation, Rivista Italiana di Geotecnica, **51**(3), 7–21, (2017). https://doi.org/10.19199/2017.3.0557-1405.07
31. E. Yesilnacar and T. Topal, Landslide susceptibility mapping: A comparison of logistic regression and neural networks methods in a medium scale study, Hendek region (Turkey), Eng Geol, **79**(3–4), 251–266 (2005). https://doi.org/10.1016/j.enggeo.2005.02.002
32. M. P. Tsai, Y. C. Hsu, H. C. Li, H. M. Shu, and K. F. Liu, Application of simulation technique on debris flow hazard zone delineation: A case study in the Daniao tribe, Eastern Taiwan, Natural Hazards and Earth System Science, **11**(11), 3053–3062, (2011). https://doi.org/10.5194/nhess-11-3053-2011
33. Y. H. Wu, K. F. Liu, and Y. C. Chen, Comparison between FLO-2D and Debris-2D on the application of assessment of granular debris flow hazards with case study, J Mt Sci, **10**(2), 293–304, (2013). https://doi.org/10.1007/s11629-013-2511-1
34. Y. C. Hsu and K. F. Liu, Combining TRIGRS and DEBRIS-2D models for the simulation of a rainfall infiltration induced shallow landslide and subsequent debris flow, Water (Switzerland), **11**(5), (2019). https://doi.org/10.3390/w11050890
35. K. F. Liu and M. C. Huang, Numerical simulation of debris flow with application on hazard area mapping, in Computational Geosciences, 221–240, (2006). https://doi.org/10.1007/s10596-005-9020-4